


Article

Surface-Response Analysis for the Optimization of a Carbon Dioxide Absorption Process Using [hmim][Tf₂N]

Grazia Leonzio ^{1,*}  and Edwin Zondervan ²

¹ Department of Industrial and Information Engineering and Economics, University of L'Aquila, Via Giovanni Gronchi 18, 67100 L'Aquila, Italy

² Laboratory of Process Systems Engineering, Department of Production Engineering, Universität Bremen, Leobener Str. 6, 28359 Bremen, Germany; edwin.zondervan@uni-bremen.de

* Correspondence: grazia.leonzio@graduate.univaq.it

Received: 2 August 2020; Accepted: 17 August 2020; Published: 1 September 2020



Abstract: The [hmim][Tf₂N] ionic liquid is considered in this work to develop a model in Aspen Plus[®] capturing carbon dioxide from shifted flue gas through physical absorption. Ionic liquids are innovative and promising green solvents for the capture of carbon dioxide. As an important aspect of this research, optimization is carried out for the carbon capture system through a central composite design: simulation and statistical analysis are combined together. This leads to important results such as the identification of significant factors and their combinations. Surface plots and mathematical models are developed for capital costs, operating costs and removal of carbon dioxide. These models can be used to find optimal operating conditions maximizing the amount of captured carbon dioxide and minimizing total costs: the percentage of carbon dioxide removal is 93.7%, operating costs are 0.66 million €/tonCO₂ captured (due to the high costs of ionic liquid), and capital costs are 52.2 €/tonCO₂ captured.

Keywords: CO₂ capture; ionic liquid; process simulation; statistical analysis; optimization

1. Introduction

Greenhouse gas emissions are mainly produced by power plants, and attention is focused on carbon dioxide reduction from these systems, in accordance with COP21 [1–3]. Generally, three strategies of carbon dioxide capture are used: pre-combustion capture, oxy-combustion capture and post-combustion capture [4–6]. Each of them entails different capture technologies (absorption, adsorption, membrane separation, etc.), and absorption is the most frequently used technology for carbon dioxide capture from flue gases [7,8]. Even if several solvents can be used, monoethanolamine (MEA) is the most widely used due to its high reactivity, low cost, good absorption capacity, and high affinity to carbon dioxide [9]. On the other hand, different disadvantages are present, such as corrosion, high energy consumption, with the associated environmental impact, and the loss of solvent [10,11].

For these reasons, the development of a sustainable and cost-competitive solvent is needed. Ionic liquids (ILs) are salts with melting points below 100 °C [12]. ILs have been investigated and developed because they can be considered to be green solvents, due to their low volatility (eliminating the possibility of gaseous emissions), good thermal and chemical stability, high selectivity towards carbon dioxide, and nonflammable and tunable structure for meeting process conditions due to the large combination of anions and cations, i.e., the theoretically available number of ILs is in the order of 10¹⁶ [2,13–15].

These properties make it possible to reduce the losses of solvent and energy for regeneration [16,17]. Moreover, the solubility values of carbon dioxide in some ILs are similar to those in MEA solutions;

for example, for [bmim][BF₄], the solubility is 0.444 at 39.7 bar and 323.15 K [9,18]. This suggests that these solvents are a good alternative to MEA solutions [19–23] for carbon dioxide capture at large scale for chemical [24] or physical absorption [25]. Generally, physical absorption is preferred for high carbon dioxide partial pressure (e.g., pre-combustion capture), while chemical absorption is suited to low carbon dioxide partial pressure (e.g., post-combustion capture) [26]. However, ILs are expensive, have slower kinetics compared to MEA solutions, and a viscosity that reduces the mass transfer kinetic [27,28]. In addition, the low volatility of ILs poses challenges in their regeneration.

Actually, most of the studies about ILs concern materials synthesis, laboratory experiments, molecular simulation, screening methodologies and phase equilibrium predictions [29]. In recent years, there has been interest in the use of COSMO-RS model to screen [bmim][NTf₂] as a potential IL among 90 classes of ILs based on carbon dioxide solubility, carbon dioxide/methane selectivity, toxicity and viscosity [30]. A new systematic and efficient screening method for IL selection was suggested by Zhao et al. [31], in addition to some solubility data of gases on ILs calculated through COSMO-RS methodology. Similarly, this method, in combination with UNIFAC, was used to predict the solubility of gases in ILs [32]. IL screening for the design of a shale gas separation process was suggested by Liu et al. [33]. Other studies have been suggested in the literature.

Zhang et al. [34] experimentally compared the energy consumption of seven ionic liquids ([emim][NTf₂], [b][BF₄], [bmim][PF₆], [bmim][NTf₂], [hmim][NTf₂], [Bmpy][NTf₂], and [Hmpy][NTf₂]) with a commercial absorbent for carbon dioxide capture: these showed lower values, and in particular, [Hmpy][NTf₂] had the lowest energy consumption under the considered operating conditions.

The influence of the thermophysical properties of IL structures on process performance are also interesting, as evaluated by Mota-Martinez et al. [35] on the basis of the non-monetized (the height of the absorption column, the area of the heat exchangers, and the heat and work requirements of the process) and monetized (annualized capital expenditure, operating expenditure, and total annual cost) key process indicators. In the same context, Valencia-Marquez et al. [2] developed a mixed integer non-linear program designing the optimal structure of an ionic liquid for carbon dioxide capture from post-combustion flue gas. It was found that the [C₁₀mim][TfO] could recover 97.65% of carbon dioxide from flue gas.

There is a clear incentive to develop capture technologies using ILs, as many recent studies have focused on process modelling and simulation. Shiflett et al. [36] compared a process for capturing carbon dioxide using MEA with one using the ionic liquid [bmim][Ac], chosen based on the chemical absorption behavior through a simulation in Aspen Plus[®]. Both processes could remove a greater amount of carbon dioxide (more than 90%) from post combustion flue gas with a high purity (higher than 95%). However, for the IL process, energy losses were 16% lower than those of the conventional MEA technology.

Basha et al. [37] developed an interesting process for carbon dioxide capture from a shifted warm flue gas, produced in a coal power plant located in Pittsburgh (USA). In the system, there were four parallel adiabatic absorbers, three flash drums placed in series for solvent regeneration, refrigerators and compressors to purify carbon dioxide sent to the storage. The [hmim][Tf₂N] was used as ionic liquid for the physical absorption of carbon dioxide. Through a simulation in Aspen Plus[®], it was found that the process could capture 95.12 mol% of carbon dioxide, with the minimum losses of solvent.

In Basha et al. [38], a process for capturing carbon dioxide from the shifted warm flue gas of a coal power plant was developed and simulated. The process had four parallel adiabatic packed bed absorbers, three flash drums in series for solvent regeneration, and two pressure/intercooling systems to separate and pressure carbon dioxide. TEGO IL K5 and TEGO IL P51P were the two ionic liquids used, and the results showed that they were able to capture respectively 91.28% and 90.59% of the carbon dioxide from flue gas.

Another physical absorption capture process was modelled by de Riva et al. [39], and its operating costs (OPEX) optimized, using the [emim][NTf₂] ionic liquid; under optimal operating

conditions, the total required energy was 1.4 GJ/ton CO₂, which is lower than that required by other capture technologies.

Ma et al. [9] simulated a new process in Aspen Plus[®] for carbon dioxide capture by using two ionic liquids: [bmim][BF₄] and [bmim][PF₆]. Compared to the convention MEA process, the energy consumption in the system using [bmim][BF₄] and [bmim][PF₆] was reduced respectively by 26.7% and 24.8%. Additionally, no problems of solvent loss and corrosion were present. In another work, Ma et al. [17] compared a capture process using [bmim][Tf₂N] with one using MEA solution: the first case made it possible to save 30.01% of energy consumption and 29.99% of primary costs. Nguyen and Zondervan [40] compared the system capturing carbon dioxide from flue gas using MEA with one using [bmim][Ac], finding that the first was economically preferable at high flue gas flow rates and carbon dioxide contents. Additionally, better conditions for an IL compared to an MEA solution were present when the partial pressure of carbon dioxide was low, such as in a post-combustion flue gas.

Mixture of ILs has also been considered in the literature. A mixture of ionic liquids and traditional solvents was analyzed by Taheri et al. [41] for carbon dioxide capture. Results show that low energy consumption and solvent losses with a high carbon dioxide capture rate were possible using pure [Amim][Tf₂N] at low or high temperature, or mixed with methanol at low temperature. Similarly, based on a simulation analysis, Huang et al. [27] found that a mixture of [Bpy][BF₄] and MEA could reduce the overall energy penalty and capture costs respect to a conventional MEA capture system by 12% and 13.5%, respectively. The same ionic liquid mixed with an aqueous solution of MEA at 30 wt% was considered by Zacchello et al. [42]. They found via simulation of the capture process that a mixed aqueous solvent with 5–30 wt% of [Bpy][BF₄] and 30 wt% of MEA led to a specific regeneration energy of 7–9% and 12–27%, respectively, and a solvent recirculation rate lower than that of MEA at 30 wt%. These advantages were also demonstrated by Yang et al. [43]; mixing 30 wt% of MEA, 40 wt% of [bmim][BF₄], and 30 wt% of H₂O, it was possible to reduce the energy consumption by 37.2% compared to an aqueous solution of MEA. An optimal ratio between the IL and the traditional solvent exists, as found by Taimoor et al. [44] when considering [bmim][MS] and MEA in their carbon dioxide capture process, developed in Aspen Hysys[®].

Other works have been focused on a single IL. Xie et al. [45] suggested that if an IL were regenerated with the reduction of pressure at a fixed temperature, [emim][EtSO₄] would ensure the lowest energy consumption; if IL were regenerated by increasing temperature at a fixed pressure, [emim][PF₆] would have the lowest energy consumption; while if IL were regenerated combining the previous techniques, [bmim][Tf₂N] would be the best solution. Zubeir et al. [46] reported that this last technology, combining pressure and temperature swing, has energetic and economic advantages for [C₆mim][TCM] ionic liquid.

In addition to physical absorption, it is possible to capture carbon dioxide via chemical absorption. Chemical absorption with ionic liquids was modelled by de Riva et al. [1] using [P2228][CNPyr] and [P66614][CNPyr]; lower energy is required with respect to other technologies reported in the literature.

In Wang et al. [47], the Rectisol process was compared to one using ionic liquids and was modelled in Aspen Plus[®]. [bmim][Tf₂N] was able to simultaneously capture CO₂ and H₂S from syngas, generated in a Texaco gasifier, although with a physical absorption and an efficiency of 97.6% and 95.3%, respectively. Operating at room temperature, the suggested system could also reduce the energy used for the refrigeration compared to the Rectisol technology, meaning that the latter could be replaced by a method using ionic liquid for industrial applications.

A mathematical model of the carbon dioxide capture process using an ionic liquid was also suggested in the literature and developed by Zareiekordshouli et al. [48] and Zhai and Rubin [29,49], along with a calculation of the energy consumption and costs. In the first, the results demonstrated that the energy requirement for a carbon dioxide capture IL-based process was about 4890 kW or 2.75 GJ/t CO₂. In the second, the cost of carbon dioxide avoided by the IL-based capture system was estimated to be \$62/t CO₂.

The above discussion suggests that the current studies discuss solubility analysis, simulation or mathematical modeling of capture process of carbon dioxide from flue gas, evaluating only costs and energy consumptions to underline the advantages of ionic liquids as compared to traditional capture solvents. No studies considering ANOVA analysis and response surface methodology (RSM) to optimize the process have been reported for these kinds of processes; this provides novelty to this research.

These methodologies are powerful because they are able to identify significant parameters inside the capture process that can be changed in order to optimize the system from an economic and environmental point of view.

In this contribution, firstly, a simulation of the process for capturing carbon dioxide from flue gas with the 1-n-hexyl-3-methylimidazolium bis(trifluoromethylsulfonyl)amide ([hmim][Tf₂N]) ionic liquid is carried out, leading to an optimization of the system, minimizing costs and maximizing the amount of captured carbon dioxide through the response surface methodology. Aspen Plus[®] is used for the simulation, while Minitab is used for the response surface methodology. The statistical tool is used to identify the significant factors of the process (even if these are well known for traditional absorption processes, they are not predictable for processes using an IL which can be subsequently correlated with performance criteria (such as costs and efficiency). These polynomial equations can be optimized to find the best operating and/or design settings. Due to the several design variables and multiple responses (objectives), the RSM and ANOVA analyses, with the latter being applied to discriminate the analysis of the former, were substituted for the computationally expensive Aspen Plus[®], which was used only to model the process.

In fact, in this analysis, the inlet temperature of flue gas, absorption column pressure, carbon dioxide composition of flue gas, and height of absorption column are the considered factors, while the percentage of carbon dioxide removal, operating costs and capital costs (CAPEX) are the analyzed responses. Important and interesting results are obtained, underlining again the novelty of this work.

The proposed method for the modeling of the process and its optimization can be extended to other ILs when their specific data are provided in order to characterize the model. Then it will not be redundant for other ILs.

2. Materials and Methods

2.1. Description of the Capture Process

The model of the process is developed in Aspen Plus[®] (Version 10, Aspen Technology, Houston, TX, USA) to capture carbon dioxide from flue gas through physical absorption with [hmim][Tf₂N] ionic liquid and is shown in Figure 1. [hmim][Tf₂N] is selected as the IL of study due to its stability, low viscosity, low water solubility and easy preparation [50,51]. Thus, it can be considered an optimal IL.

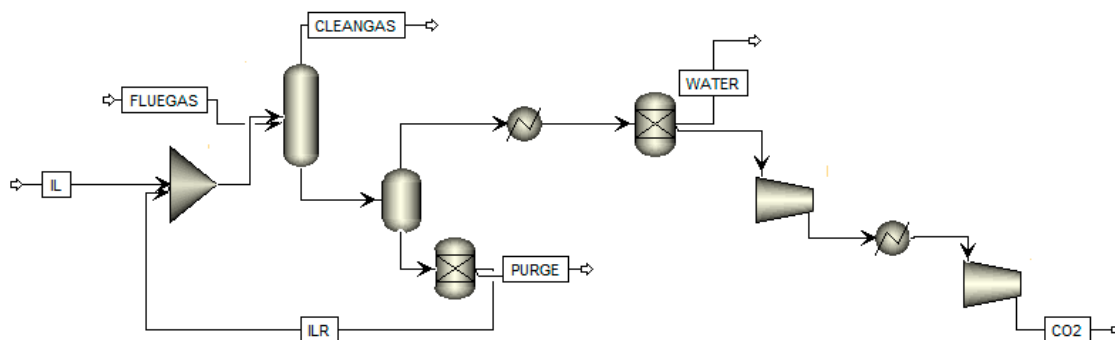


Figure 1. Process scheme of carbon dioxide absorption process from flue gas with IL in Aspen Plus[®] environmental.

The overall process contains a packed bed absorber, one flash for IL regeneration with the pressure swing option, a pressure intercooling system for separating carbon dioxide from water, and finally compressors with intercooling to increase the pressure of the captured carbon dioxide. In the system, carbon dioxide is captured, in particular, from a shifted warm pre-combustion flue gas produced by an industrial coal power plant (400 MWe) in Pittsburgh [37]. The characterization of the considered flue gas is reported in Table 1. Generally, the temperature and pressure of feed are respectively of 500 K and 30 bar with an industrial flow rate of 25.63 kg/s. The same feed flow rate of the work of Basha et al. [37] is taken into account.

Table 1. Composition of the analyzed flue gas [37].

Component	mol%
Ar	0.48
CH ₄	0.24
H ₂	37.5
N ₂	0.33
CO	6.27
CO ₂	23.87
H ₂ O	30.68
NH ₃	0.16
H ₂ S	0.47

For the physical absorption with [hmim][Tf₂N], a Rate-Based model (RADFRAC) is considered: the gas-solvent mass transfer in the packed bed column is modeled by the Billet and Schultes's correlation, valid for a column with a random and structured packing as the following equations (see Equations (1) and (2)) [52,53]:

$$k_L = C_L \cdot 12^{1/6} \cdot \sqrt{\frac{D_L \cdot u_{Ls} \cdot a_p}{4 \cdot \varepsilon \cdot h_L}} \quad (1)$$

$$h_L = \left(12 \cdot \frac{u_{Ls} \cdot a_p^2 \cdot \mu_L}{\rho_L \cdot g} \right)^{\frac{1}{3}} \quad (2)$$

where a_p is the specific geometric area of packing, D_L is the liquid phase diffusion coefficient, u_{Ls} is the superficial liquid velocity, ε is the packing porosity, C_L is a parameter of 0.905, μ_L is the liquid viscosity, h_L the operating liquid hold up, g gravity acceleration. The considered column is a packed bed absorber, filled with plastic pall rings with a dimension of 50 mm, a packing surface area of 110 m²/cm³ and 10 stages with a dimension of 3 m, then the total height of the column is 30 m. The void fraction is 0.93. The packed column diameter is 5.5 m and is chosen to avoid flooding inside the column: it operates at 70% of the critical flooding conditions [40]. The shifted flue gas enters from the bottom of the column, while the ionic liquid enters from the top, with a flow rate of 260 kg/s, counter-currently. At a fixed flue gas flow rate, the amount of IL is calculated to capture carbon dioxide. In this condition, 90% of carbon dioxide is captured to be used/stored. From the absorber, two currents are obtained: the gas stream (IL-poor) from the top, rich in hydrogen, and the liquid stream (IL-rich) from the bottom.

The IL-rich stream is regenerated with a pressure swing option using an adiabatic flash at a pressure of 1 bar. From this operation, a carbon dioxide gas stream, also containing some water vapor, and an IL solvent-rich stream are produced. The latter, from the bottom of the flash, is pumped, heated and recycled to the absorber column. The first stream, from the top of the flash, is cooled to 288 K to separate water. The resulting stream, rich in carbon dioxide, is then compressed with an inter-refrigeration stage to 150 bar for transportation, use and/or storage.

The economic analysis of the process is developed through the use of Aspen Process Economic Analyzer (APEA) evaluating the operating and capital costs over the 20 years of life, with an interest rate of 10%. Total costs are the sum of OPEX and CAPEX costs. Regarding the capital costs, the

equipment cost for each component is calculated using Aspen In-Plant Cost Estimator [54]. In any case, CAPEX costs include direct and indirect costs. The operating costs instead include the total costs of raw materials, utilities, operating labor, maintenance, operating charges, plant overhead and general and administrative expenses. Regarding the utilities, the costs of steam, cooling water, electricity and ionic liquid are, respectively, 8.93 €/GJ, 0.32 €/GJ, 0.15 €/kWh and 18.16 €/kg [40].

The green ionic liquid [hmim][Tf₂N], with the chemical formula of C₁₂H₁₉F₆N₃O₄S₂, has been of interest within the scientific community due to its stability, low viscosity, low water affinity and easy of synthesis. Its molecular structure is shown in Figure 2 [37], while the elemental chemical analysis according to the IUPAC is shown in Table 2 [55].

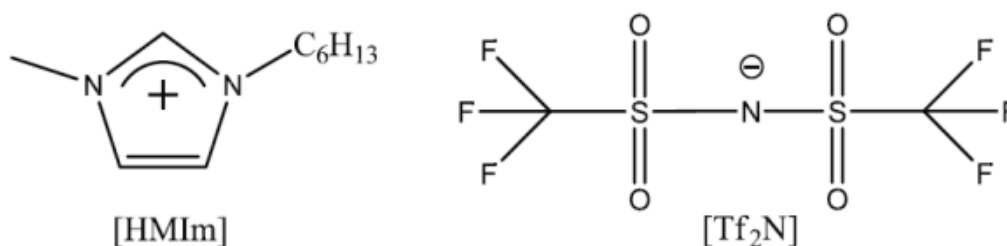


Figure 2. Molecular structure of the considered ionic liquid [hmim][Tf₂N] [37].

Table 2. Elemental chemical analysis of [hmim][Tf₂N] ionic liquid according to the IUPAC [55].

C.%	32.21
H.%	4.28
N.%	9.39
F.%	25.48
S.%	14.33

The solubility of carbon dioxide in this ionic liquid has already been investigated (see [55–57]). These authors found that at a fixed pressure, an increase in temperature causes a reduction in carbon dioxide solubility in [hmim][Tf₂N]; then, when pressure and temperature are 3 MPa and 293.15 K (413.2 K), about 3 (0.55) mol of carbon dioxide is dissolved in one kilogram of [hmim][Tf₂N] [57].

These data are used to find the expression for Henry's constant of carbon dioxide in this IL. Initially, it is considered that Henry's law constant at the vapor pressure of the solvent (P_{IL}^{sat}) k_{H,CO_2}^0 has the following relation (see Equation (3)) [57,58]:

$$\ln(k_{H,CO_2}^0) = 7.3141 - \frac{1838.8}{T} + 0.002809 \cdot T \quad (3)$$

where T is temperature. Then, the Henry's law at a fixed pressure and temperature for carbon dioxide in the selected ionic liquid based on the molality scale is the following (see Equation (4)):

$$k_{H,CO_2} = k_{H,CO_2}^0 \cdot e^{\frac{V_{m,CO_2}^\infty \cdot P}{R \cdot T}} \quad (4)$$

where P is pressure, T is temperature, R is the universal gas constant, and V_{m,CO_2}^∞ is the partial molar volume of carbon dioxide at infinite dilution, according to the following equation [37] (see Equation (5)):

$$V_{m,CO_2}^\infty = -162.8 + 0.1365 \cdot T \quad (5)$$

where T is temperature. With these relations, it is possible to define the real fugacity of carbon dioxide in the liquid phase according to the following relations (see Equations (6) and (7)) [37]:

$$f_{CO_2,L} = k_{H,CO_2} \cdot \frac{m_{CO_2}}{m^0} \cdot \gamma_{CO_2}^* \quad (6)$$

$$\gamma_{CO_2}^* = e^{2 \cdot \frac{m_{CO_2}}{m^o} \cdot (0.20914 - \frac{72.12}{T})} \quad (7)$$

where $\gamma_{CO_2}^*$ is the carbon dioxide activity coefficient, m_{CO_2} is carbon dioxide solubility expressed in mol_{CO₂}/kg_{IL}, m^o is equal to 1 mol/kg, and T is temperature.

For the simulation in Aspen Plus[®], the ionic liquid [hmim][Tf₂N] is inserted as a new component, defining the expression of density (ρ) in kg/m³, viscosity (μ_L) in Pas, surface tension (σ_L) in N/m, vapor pressure (P^v) in Pa, heat capacity (C_p) in J/molK as a function of temperature T in K (see Equations (8)–(12)) [37]:

$$\rho = 1635.89 - 0.8892 \cdot T \quad (8)$$

$$\mu_L = 0.658455 \cdot e^{\frac{123792843.733183}{T^3}} \quad (9)$$

$$\sigma_L = 13.31644 - \frac{5433.9922}{T} \quad (10)$$

$$\ln(P^v) = 28.31918 - \frac{14848.95148}{T} \quad (11)$$

$$C_p = 0.64550 \cdot T - 439.27 \quad (12)$$

To define the IL, critical properties as critical pressure and temperature [59], acentric factor, critical volume and critical compressibility factor [60] are also defined, as shown in Table 3.

Table 3. Critical properties for the ionic liquid [hmim][Tf₂N].

Critical temperature	815	K
Critical pressure	16.11	bar
Acentric factor	0.8556	
Critical volume	1104.4	cm ³ /mol
Critical compressibility factor	0.2626	

The molecular weight of [hmim][Tf₂N] is 447.42 g/mol [61] 2018.

2.2. Thermodynamic Model

According to a coefficient fugacity approach for the equilibrium calculation, the thermodynamic model that is used to simulate the process is the Peng Robinson using the Boston-Mathias alpha function and mixing rules; in fact, this model provides reasonable results at all temperatures and pressures, even at high pressures. In addition to the binary interaction parameters, critical properties and acentric factor are also required.

This model is widely used in the petroleum and chemical industries due to its simplicity and accuracy [62–64].

Moreover, it has also been used for the description of processes involving ionic liquids at different temperatures and pressures [65].

The equation of state is the following (see Equation (13)):

$$P = \frac{R \cdot T}{v_m - b} - \frac{a}{v_m \cdot (v_m + b) + b \cdot (v_m - b)} \quad (13)$$

where P is pressure, R is universal gas constant, T is temperature, and v_m is the molar volume of mixture, while b and a functions are expressed respectively by the following relations (see Equations (14) and (15)):

$$b = \sum_i x_i \cdot b_i \quad (14)$$

$$a = a_0 + a_1 \quad (15)$$

where b_i is calculated for each component according to the respective critical temperature and pressure [66], x_i is the molar fraction of i component in the mixture, while for the so-called a function, the following relations for the standard quadratic mixing rule term, a_0 , and for the additional asymptotic term, a_1 , used to model highly nonlinear systems are taken into account (see Equations (16)–(19)) [37]:

$$a_0 = \sum_i \sum_j x_i x_j (a_i a_j)^{0.5} (1 - \delta_{i,j}) \quad (16)$$

$$\delta_{i,j} = \delta_0 + \delta_1 \cdot T + \frac{\delta_2}{T} \quad (17)$$

$$a_1 = \sum_i x_i \left(\sum_j x_j \left[(a_i a_j)^{0.5} l_{i,j} \right]^{\frac{1}{3}} \right)^3 \quad (18)$$

$$l_{i,j} = l_0 + l_1 \cdot T + \frac{l_2}{T} \quad (19)$$

where a_i and a_j for each component are a function of temperature, critical temperature and pressure and acentric factor, x_i and x_j are the molar fraction in the mixture for component i and j , respectively, $\delta_{i,j}$ and $l_{i,j}$ are binary interaction parameters as a function of temperature and other parameters (l_0 , l_1 , l_2 and δ_0 , δ_1 , δ_2). For these binary interaction parameters, it can be considered that $\delta_{i,j} = \delta_{j,i}$ while $l_{i,j} = l_{j,i}$.

Table 4 shows the values of binary interaction parameters between the ionic liquid [hmim][Tf₂N] and other components of the mixture. These values are obtained by fitting experimental solubility data, as shown in Table 5 for carbon dioxide [37].

Table 4. Binary parameter interactions for the [hmim][Hf₂N] ionic liquid according to Equations (15) and (17).

Binary	δ_0	δ_1	δ_2	l_0	l_1	l_2
IL-CO ₂	5.338×10^{-2}	-3.46×10^{-4}	2.3685	-0.81206	1.01×10^{-3}	113.665
IL-H ₂	-1.4121	1.7344×10^{-3}	2.4150×10^2	-4.9770×10^{-1}	1.0679×10^{-3}	1.0603×10^2
IL-CH ₄	1.4941	-2.5628×10^{-3}	-2.0970×10^2	-2.0888	3.5794×10^{-3}	3.2669×10^2
IL-CO	1.1728	-3.2704×10^{-3}	-1.0312×10^2	-1.0052	2.9159×10^{-3}	1.0964×10^2
IL-H ₂ S	8.789×10^{-1}	-1.5492×10^{-3}	-1.3364×10^2	-4.9490×10^{-1}	1.7573×10^{-3}	-3.3794×10^{-3}

Table 5. Solubility data of CO₂ in the ionic liquid [hmim][Tf₂N] at 298.1 K [37].

Pressure (bar)	Solubility (molCO ₂ /kg[IL])
80	8.94
51	5.21
37	3.35
26	2.23
18	1.49
11	0.958
8	0.558
2	0.248
0	0

As provided in the work of Basha et al. [37], good agreement is present between the experimental (reported in Shiflett and Yokozeki [55], Ren et al., [59] and Kumelan et al. [57]) and predicted gas solubilities in the ionic liquid [hmim][Tf₂N].

For the other binaries, the default values of binary interactions present in Aspen Plus[®] are considered.

2.3. Response Surface Methodology

Response surface methodology is a statistical methodology first suggested by Box and Wilson for the analysis of experimental data [67]. Now, this method is applied for optimization, parameter configuration and observation design. This methodology is used in conjunction with central composite design (CCD), and is useful without a large number of design points [68]. In fact, only 2^k factorial tests, 2^k star tests, n_c center point tests and replication tests are required, with k being the number of factors.

A model correlating the response and the influencing factors and interactions is obtained, and the general form of this response surface equation is the following [69] (see Equation (20)):

$$Y = \beta_0 + \sum_{i=1}^k \beta_i x_i + \sum_{i=1}^k \beta_{ii} x_i^2 + \sum_{i < j} \beta_{ij} x_i x_j + e(x_1, x_2, \dots, x_k) \quad (20)$$

where Y is the considered response, x_i is the independent variable, β_i , β_{ii} , β_{ij} are the regression coefficients of linear, quadratic and interaction terms, respectively, k is the number of influencing factors, and e is the error. It is a second-degree polynomial, for which the significance of factors and interactions is verified by using the ANOVA analysis through Yate's algorithm.

In our work, the star points are set on the center of each face of the factorial face, then the value of α (the distance between the central and star points) is 1. This particular design is known as face-centered central composite design (FCCCD). Four factors are considered: the flue gas inlet temperature, column pressure, carbon dioxide composition in flue gas and the height of the absorber, as shown in Table 6.

Table 6. Values of each level for each factor in the FCCCD analysis.

Code	Factor	Level		
		(−1)	0	(+1)
A	Flue gas inlet temperature (K)	323	411.5	500
B	Column pressure (bar)	15	22.5	30
C	CO ₂ composition in flue gas (mol%)	3	13.5	24
D	Height of the absorber (m)	2	26	50

Considering that 4 factors, 16 factorial tests, 8 star tests, 6 central tests and 1 replication test are carried out, then overall 31 simulations are executed in Aspen Plus®. The percent of carbon dioxide removal from flue gas, operating and capital costs are the analyzed responses.

Minitab software is used for regression, graphical analysis, statistical analysis, and optimization of the selected responses. The optimization of the system is carried out by the desirability approach.

3. Results and Discussion

3.1. Results of Process Simulation

The simulation is carried out in Aspen Plus®. At first the model is validated by using a flash and obtaining the solubility data provided in the work of Basha et al. [37] at different temperatures and pressures.

The material and energy balances are found according to the conditions set in the previous section. Table 7 shows the results for the inputs and outputs of the process, according to the flowsheet proposed in Figure 1.

The process treats 25.63 kg/s of shifted flue gas with 260 kg/s of ionic liquid through physical absorption. The process is able to produce 13.65 kg/s of carbon dioxide stream that can be stored or used at a pressure of 153 bar. Additionally, it is possible to recover 90% of carbon dioxide from the shifted flue gas. No flooding problems are present for the absorber. The considered process costs 27 million€ for the capital costs and 0.335 trillion€/year for the operating costs. It is clear that the

extremely high operating costs are due to the high cost of the ionic liquid, the quantity of which is calculated to treat an industrial amount of flue gas. Compared to a pilot plant, an industrial plant capturing carbon dioxide with ILs has higher operating costs due to the higher value of the IL flow rate, which is characterized by high costs [39].

Table 7. Material and energy balances for inputs and outputs obtained for the simulation of carbon dioxide capture process in Aspen Plus®.

	Flue Gas	IL	Clean Gas	Water	CO ₂
Temperature (K)	500	468	468	288	223
Pressure (bar)	30	30	30	28	150
Vapor fraction	1	0	1	0	1
Molar enthalpy (kcal/mol)	-40.35	17.25	-8.42	-68.87	-70.77
Total mass flow rate (kg/s)	25.63	260	4.66	7.09	13.65
Ar (kg/s)	0.26	0	0.20	0	0.06
CH ₄ (kg/s)	0.05	0	0.03	0	0.02
H ₂ (kg/s)	1.01	0	0.87	0	0.17
N ₂ (kg/s)	0.12	0	0.10	0	0.02
CO (kg/s)	2.36	0	1.87	0	0.49
CO ₂ (kg/s)	14.13	0	1.4	0	12.67
H ₂ O (kg/s)	7.43	0	0.16	7.09	0
NH ₃ (kg/s)	0.04	0	0	0	0.03
H ₂ S (kg/s)	0.22	0	0	0	0.21
IL (kg/s)	0	260	0	0	0

It is interesting to analyze the ratio between the fugacity of carbon dioxide in the liquid phase and carbon dioxide solubility in IL for a real solution.

Figure 3 shows this ratio as a function of pressure in the range between 0 bar and 80 bar for a temperature set at 298.15 K; with increasing pressure, this ratio decreases (a higher solubility of carbon dioxide should be achieved in the ionic liquid).

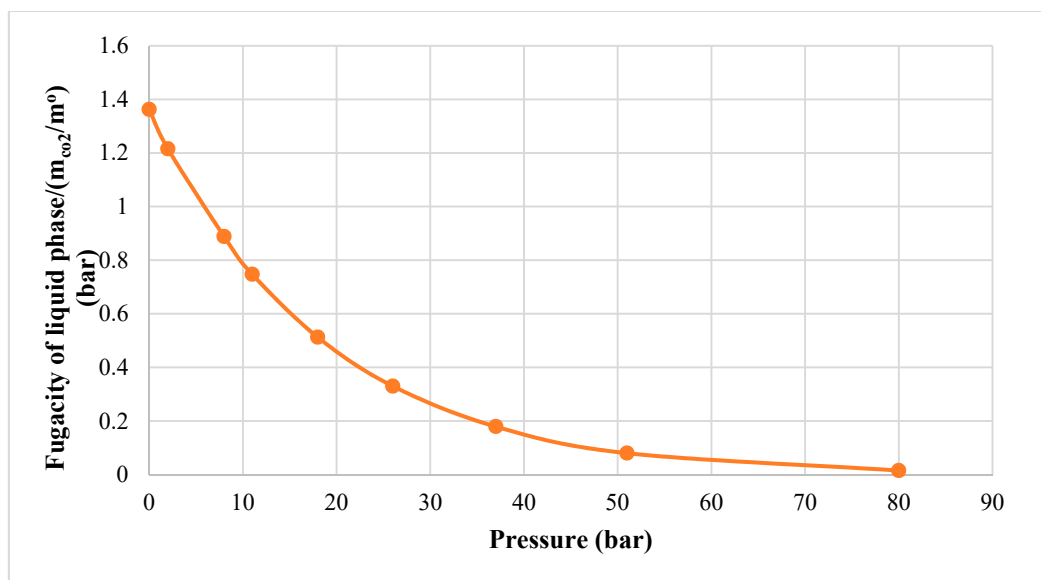


Figure 3. Ratio between the fugacity of carbon dioxide in the liquid phase and carbon dioxide solubility as a function of pressure for a real solution at 298.15.

3.2. Results of the Response Surface Methodology

Thirty-one different simulations are carried out according to the face-centered central composite design considering the process model developed in Aspen Plus®. As mentioned before, the output

data from these tests are used to find a mathematical expression for the analyzed responses, like the percentage of carbon dioxide removal, and CAPEX and OPEX costs.

At first, the significance of the fit for the second-order polynomials of these responses is estimated using analysis of variance (ANOVA). The results are given in Table 8; the significance of each term is evaluated, as well as the effect of single terms and their interactions on the considered responses.

The statistical significance is verified by the F -value (Fischer variation ratio) and p -value (significant probability value) [70]. Each coefficient inside the mathematical model is significant if the value of its probability is higher than F ; model terms with a p -value lower than 0.05 are significant at a 95% confidence level [71,72].

Table 7 shows that for the CAPEX costs, factors A (flue gas inlet temperature), B (column pressure) and D (height of the absorber) are significant. In particular, the first factor has a negative effect on the considered response, while factors B and D have a positive effect. To reduce the capital costs, the inlet temperature of flue gas can be increased while reducing the column pressure and the height of the absorber.

For the OPEX costs, only interaction DD has a positive effect, and it is significant; the operating costs increase when the height of the absorber is higher.

For the third analyzed response, factors B (column pressure) and D (the height of the absorber), with the second-order interactions BC, BD, CD, BB are significant. Factor B has a positive effect, while factor D has a negative effect on the response. The second-order interactions, with the exception of interaction BB, all have a positive effect on the removal of emissions. To capture more carbon dioxide, it is better to increase pressure inside the absorber and reduce its height.

Overall, factors B, C and D influence the process in a stronger way, while factor A is only significant only for the capital costs.

The following quadratic polynomial equations are proposed relating the responses to the influence factors (see Equations (21)–(23)):

$$CAPEX (\text{€}) = 22,370,478 - 427,029 \cdot A + 1,076,170 \cdot B + 1,288,803 \cdot D \quad R^2 = 91\% \quad (21)$$

$$OPEX \left(\frac{\text{€}}{\text{year}} \right) = 2.85 \times 10^{11} + 3.76 \times 10^9 \cdot DD \quad R^2 = 90\% \quad (22)$$

$$CO_2 \text{ removal } (\%) = 72.42 + 23.59 \cdot B + 1.13 \cdot BC + 1.02 \cdot BD + 1.02 \cdot CD - 0.91 \cdot D - 3.36 \cdot BB \quad R^2 = 99\% \quad (23)$$

where factor A is the flue gas inlet temperature, factor B is the column absorber pressure, factor C is carbon dioxide composition in flue gas and factor D is the height of column absorber. The fitness of these models is provided by the regression coefficient (R^2), suggesting a good agreement between the simulation and calculated data at high values [73,74]. Figure 4 shows the normal probability plot of residuals for the CAPEX, OPEX costs and the percentage of carbon dioxide removal: the errors are distributed normally across a straight line and are insignificant.

Table 8. Results of ANOVA analysis for the considered responses.

Source	Carbon Dioxide Removal (%)					OPEX Costs (£/year)					CAPEX Costs (£)				
	DF	SS	MS	F-Value	p-Value	DF	SS	MS	F-Value	p-Value	DF	SS	MS	F-Value	p-Value
Model	14	10,157.8	725.6	534.34	0	14	1.21×10^{20}	8.66×10^{18}	1.17	0.378	14	5.97×10^{13}	4.26×10^{12}	11.05	0
Linear	4	10,038.4	2509.6	1848.19	0	4	2.04×10^{19}	5.09×10^{18}	0.69	0.611	4	5.41×10^{13}	1.35×10^{13}	35.04	0
A	1	4	4	2.98	0.103	1	6.83×10^{18}	6.83×10^{18}	0.92	0.351	1	3.28×10^{12}	3.28×10^{12}	8.51	0.01
B	1	10,018.5	10,018.5	7378.18	0	1	6.66×10^{18}	6.66×10^{18}	0.9	0.357	1	2.08×10^{13}	2.08×10^{13}	54.04	0
C	1	0.8	0.8	0.58	0.456	1	6.89×10^{18}	6.89×10^{18}	0.93	0.349	1	3.57×10^{10}	3.57×10^{10}	0.09	0.765
D	1	15	15	11.03	0.004	1	8.91×10^{14}	8.91×10^{14}	0	0.991	1	2.99×10^{13}	2.99×10^{13}	77.51	0
Square	4	63.8	16	11.75	0	4	5.62×10^{19}	1.40×10^{19}	1.9	0.16	4	2.88×10^{12}	7.20×10^{11}	1.87	0.165
A-A	1	0	0	0.01	0.922	1	7.58×10^{18}	7.58×10^{18}	1.02	0.327	1	1.14×10^{12}	1.14×10^{12}	2.95	0.105
B-B	1	29.3	29.3	21.61	0	1	7.58×10^{18}	7.58×10^{18}	1.02	0.326	1	1.14×10^{12}	1.14×10^{12}	2.95	0.105
C-C	1	0.3	0.3	0.2	0.661	1	7.57×10^{18}	7.57×10^{18}	1.02	0.327	1	1.77×10^{11}	1.77×10^{11}	0.46	0.508
D-D	1	0.2	0.2	0.12	0.73	1	3.67×10^{19}	3.67×10^{19}	4.96	0.041	1	5.91×10^{10}	5.91×10^{10}	0.15	0.701
2-Way Interaction	6	55.7	9.3	6.83	0.001	6	4.47×10^{19}	7.44×10^{18}	1.01	0.455	6	2.75×10^{12}	4.58×10^{11}	1.19	0.361
A-B	1	1.3	1.3	0.96	0.342	1	7.42×10^{18}	7.42×10^{18}	1	0.331	1	3.79×10^{11}	3.79×10^{11}	0.98	0.336
A-C	1	0.4	0.4	0.29	0.6	1	7.51×10^{18}	7.51×10^{18}	1.02	0.329	1	7.26×10^{11}	7.26×10^{11}	1.88	0.189
A-D	1	0	0	0	0.985	1	7.43×10^{18}	7.43×10^{18}	1	0.331	1	2.75×10^{11}	2.75×10^{11}	0.71	0.411
B-C	1	20.4	20.4	15.04	0.001	1	7.56×10^{18}	7.56×10^{18}	1.02	0.327	1	4.87×10^9	4.87×10^9	0.01	0.912
B-D	1	16.8	16.8	12.39	0.003	1	7.43×10^{18}	7.43×10^{18}	1	0.331	1	1.27×10^{12}	1.27×10^{12}	3.29	0.088
C-D	1	16.7	16.7	12.31	0.003	1	7.30×10^{18}	7.30×10^{18}	0.99	0.335	1	9.57×10^{10}	9.57×10^{10}	0.25	0.625
Error	16	21.7	1.4			16	1.18×10^{20}	7.40×10^{18}			16	6.17×10^{12}	3.86×10^{11}		
Lack-of-Fit	10	21.7	2.2			10	1.18×10^{20}	1.18×10^{19}			10	6.17×10^{12}	6.17×10^{11}		
Pure Error	6	0	0			6	0	0			6	0	0		
Total	30	10,179.5				30	2.40×10^{20}				30	6.59×10^{13}			

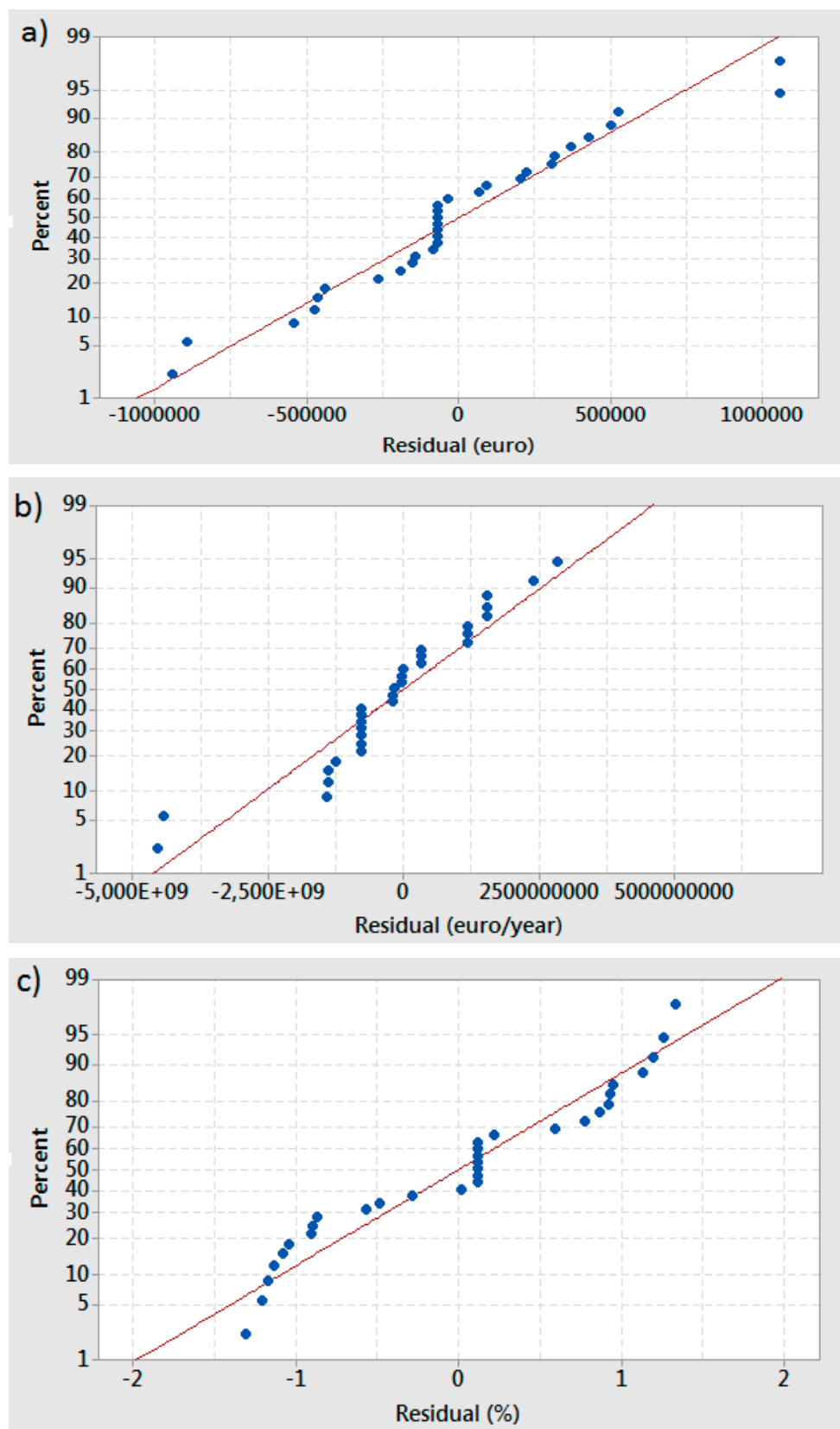


Figure 4. Normal probability plot of residual for: (a) CAPEX costs; (b) OPEX costs; (c) percentage of carbon dioxide removal.

Figures 5–7 show the surface plots of the CAPEX, OPEX and percentage of carbon dioxide removal.

In particular, Figure 5 shows the surface plots for the CAPEX costs as a function of different factors. Figure 5a shows CAPEX costs as a function of factor *C* (carbon dioxide composition in flue gas) and *D* (the height of the absorber). Factor *C* is not significant, while factor *D* has a positive effect on the response. No interactions are present between the two factors. Figure 5b shows the CAPEX costs as a function of factor *B* (column pressure) and *D* (the height of the absorber), both with a positive effect. Then, increasing the column pressure, a higher value of capital costs is obtained. Figure 5c shows CAPEX costs as a function of factor *B* (column pressure) and *C* (carbon dioxide composition in flue gas). The effect of these factors has already been discussed. No significant interactions are present between them. Figure 5d shows the CAPEX costs as a function of factor *A* (flue gas inlet temperature) and factor *D* (the height of the absorber); the first factor has a negative effect on the considered response, while the second factor has a positive effect. No significant interactions are present between factor *A* and *D*. Figure 5e shows the surface plot of the CAPEX costs as a function of factor *A* (flue gas inlet temperature), and factor *C* (carbon dioxide composition in flue gas); the first has a negative effect, while the second has a non-significant effect. No significant interactions are present. Figure 5f presents the CAPEX costs as a function of factor *A* (flue gas inlet temperature), with negative effect, and factor *B* (column pressure), with a positive effect. To reduce the CAPEX costs, it is better to work at high flue gas inlet temperatures, and at low pressures and heights of column absorber.

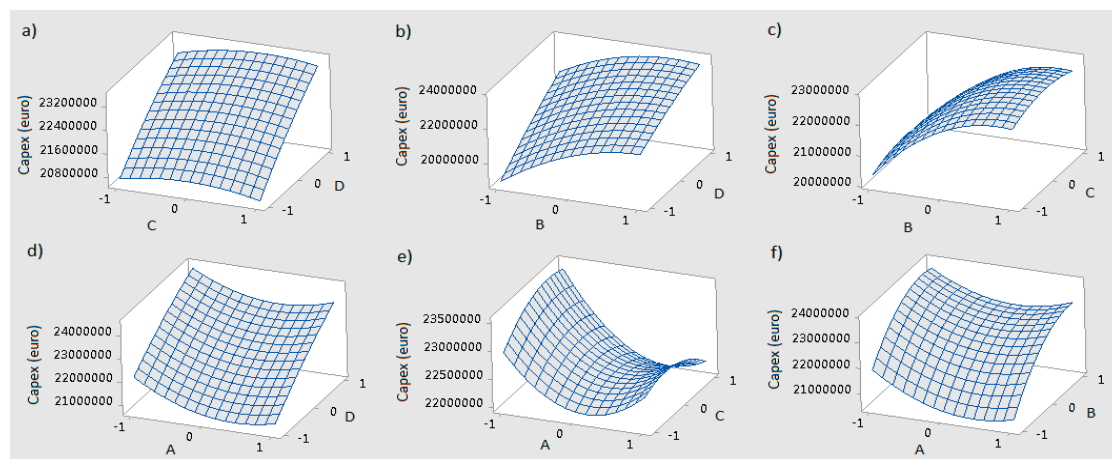


Figure 5. Response surface plots for CAPEX (€) as a function of: (a) factor *C* and *D*; (b) factor *B* and *D*; (c) factor *B* and *C*; (d) factor *A* and *D*; (e) factor *A* and *C*; (f) factor *A* and *B* (Hold values: $A = B = C = D = 0$) (factor *A* = flue gas inlet temperature, factor *B* = column pressure, factor *C* = carbon dioxide composition in flue gas, factor *D* = height of the absorber).

Figure 6 shows the surface plots for the OPEX costs as a function of different factors. Figure 6a shows the OPEX costs as a function of factor *C* (carbon dioxide composition in flue gas) and factor *D* (the height of the absorber). Due to the variation of operating costs between 0.282 trillion€/year and 0.288 trillion €/year, both factors are not significant. The same considerations are valid for factor *B* (column pressure) and factor *C* (carbon dioxide composition in flue gas), as in Figure 6b, where the surface plot of OPEX costs is reported as a function of these factors. Figure 6c shows the OPEX costs at different values of factor *B* (column pressure) and factor *D* (the height of the absorber). These costs are between 0.282 trillion€/year and 0.288 trillion€/year, and are not significant. Figure 6d presents the trend of the OPEX costs as a function of factor *A* (flue gas inlet temperature) and factor *D* (the height of the absorber), in this case, too, the small variation of operating costs suggests that these factors are not significant. Figure 6e shows the surface plot of the OPEX costs as a function of factor *A* (flue gas inlet temperature) and factor *C* (carbon dioxide composition in flue gas). No strong variations are observed when changing these factors, also the interactions are not significant. On the other hand, Figure 6f shows the operating costs as a function of factor *A* (flue gas inlet temperature) and factor *B* (column

pressure): these factors and their interaction are not significant. As shown in Equation (23), only the second-order interaction DD is significant for this response.

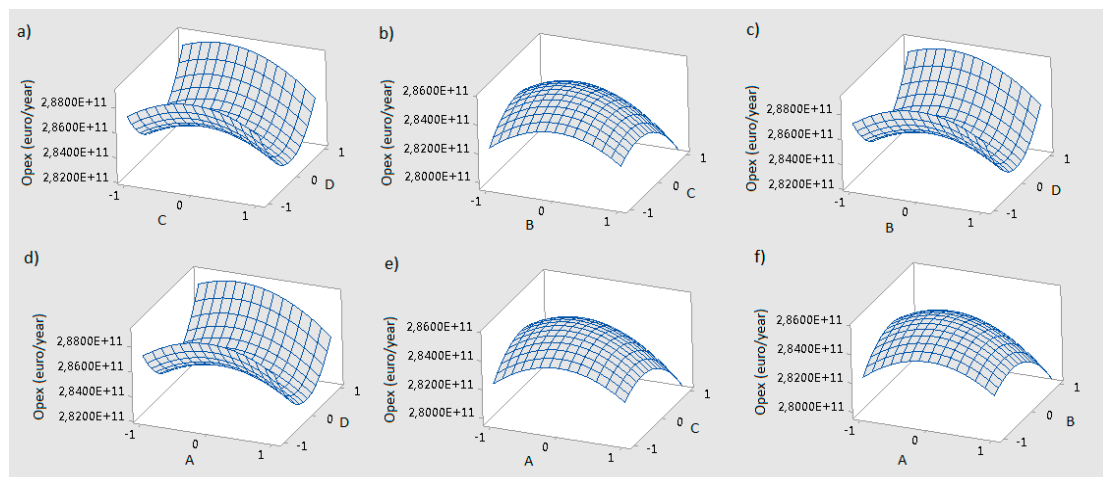


Figure 6. Response surface plots for OPEX (€/year) as a function of: (a) factor C and D; (b) factor B and C; (c) factor B and D; (d) factor A and D; (e) factor A and C; (f) factor A and B. (Hold values: $A = B = C = D = 0$) (factor A = flue gas inlet temperature, factor B = column pressure, factor C = carbon dioxide composition in flue gas, factor D = height of the absorber).

Figure 7 shows the surface plots for the percentage of carbon dioxide removal as a function of different factors.

Figure 7a shows carbon dioxide removal as a function of factor C (carbon dioxide composition in flue gas), without significant effect, and factor D (the height of the absorber), with a negative effect. However, the interaction of these factors is significant with a positive effect. Factor C, as a single factor is not significant, but becomes significant in the interaction with factor D. Figure 7b shows the surface plot of carbon dioxide removal as a function of factor B (column pressure), with a positive effect, and factor D (the height of the absorber), with a negative effect. Then it is better to increase pressure and reduce the height of column to capture more carbon dioxide. Interaction BD is also significant with a positive effect on the considered response. Figure 7c shows the amount of captured carbon dioxide as a function of factor B (column pressure) and factor C (carbon dioxide composition in flue gas). Only factor B is significant, but factor C becomes significant in the presence of factor B, in the interaction BC. This second-order interaction has a positive effect. Figure 7d shows the trend of carbon dioxide capture as a function of factor A (flue gas inlet temperature) and factor D (the height of the absorber). Only factor D is significant. Figure 7e presents the surface plot of carbon dioxide removal as a function of factor A (flue gas inlet temperature) and factor C (carbon dioxide composition in flue gas). Due to the small variations of this response, these factors are not significant. Additionally, no significant interactions are present between factor A and C. Figure 7f shows carbon dioxide removal as a function of factor A (flue gas inlet temperature) and factor B (column pressure). Only factor B is significant with a positive effect. To improve the efficiency on carbon dioxide capture, it is better to work on factor B, increasing the pressure of the absorber, and on factor D, reducing the height of the absorber. However, with increasing pressure, the capital costs are also increased, so a compromise between these two opposite trends should be found in order to have the optimal operation of the process.

The optimization of the process is developed through a desirability approach, according to the following equations (see Equation (24)):

$$D = (d_1(Y_1)d_2(Y_2)d_3(Y_3) \dots d_k(Y_k))^{1/k} \quad (24)$$

with D being the overall desirability and $d_i(Y_i)$ the desirability function of each response Y_i .

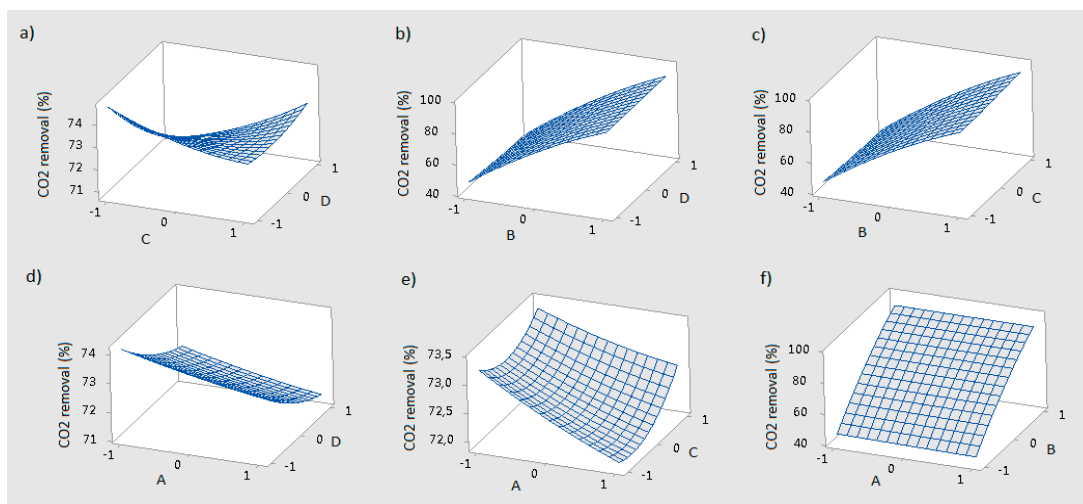


Figure 7. Response surface plots for percentage of carbon dioxide removal (%) as a function of: (a) factor C and D; (b) factor B and D; (c) factor C and B; (d) factor A and D; (e) factor A and C; (f) factor A and B. (Hold values: $A = B = C = D = 0$) (factor A = flue gas inlet temperature, factor B = column pressure, factor C = carbon dioxide composition in flue gas, factor D = height of the absorber).

Capital and operating costs are minimized, while the captured carbon dioxide is maximized. Under optimal conditions, factors A, B, C and D should be, respectively, equal to 500 K, 30 bar, 24 mol% and 1.36 m. These conditions ensure that the percentage of carbon dioxide removal is equal to 93.7%, the operating costs are 0.279 trillion€/year (0.66 million€/tonCO₂ captured), and the capital costs are 21.9 million€ (52.2 €/tonCO₂ captured).

The obtained values are comparable with other studies. Significant carbon dioxide reductions were also obtained in the work of Nguyen and Zondervan [40] and de Riva et al. [39]. Capital and operating costs were not suggested for the [him][Tf₂N] then, thus not allowing an easy comparison. However, for [bmim][Ac], [bmim][BF₄] and [bmim][PF₆], economic data can be found and suggested [9,36], but a straight comparison cannot be made with the used ionic liquid. However, from a first analysis it is possible to consider the relations proposed by Nguyen and Zondervan [40] for OPEX and CAPEX of [bmim][Ac] as a function of flue gas flow rate and carbon dioxide composition. A comparison between this work and the suggested relations of Nguyen and Zondervan [40] shows that CAPEX values are comparable, while a higher OPEX is calculated due to the required flow rate and cost of the used IL. Overall, of course, higher costs are calculated for the ionic liquid compared to the traditional MEA, as reported in the work of Ferrara et al. [75], where an average cost of 30 \$/tonCO₂ captured is considered.

4. Conclusions

In this work, a physical absorption process capturing carbon dioxide from a shifted flue gas through the ionic liquid [hmim][Tf₂N] is optimized. IL is chosen due to its better performances when compared to traditional ones.

The response surface methodology is applied to determine which factors are significant and what relationship these have with performance criteria (such as costs and carbon dioxide removal). The need to optimize the system is suggested by the high costs of ionic liquids. In particular, a face-centered central composite design is developed, and the optimal conditions are evaluated by the desirability approach. Then a methodology of optimization is suggested for the capture process by using ILs and important and interesting results are obtained.

In this work, the flue gas inlet temperature, column absorber pressure, carbon dioxide composition in flue gas, and height of the column absorber are the considered factors. The operating and capital costs and the amount of reduced carbon dioxide are considered as responses. The surface plots of these responses are found, as well as a mathematical model as a function of significant factors and

interactions. Among the results, it is found that the pressure of the absorber, the carbon dioxide composition in the flue gas, and the height of the absorber influence the process the most strongly, while the flue gas inlet temperature only influences the capital costs. From the optimal operating conditions, it is found that the flue gas inlet temperature, column absorber pressure, carbon dioxide composition in flue gas and the height of column absorber should be, respectively, 500 K, 30 bar, 24 mol% and 1.36 m. Under these conditions, the operating costs, capital costs and the percentage of carbon dioxide removal are, respectively, 0.66 million€/tonCO₂ captured, 52.2 €/tonCO₂ captured and 93.7%.

Author Contributions: Conceptualization, G.L., E.Z.; methodology, G.L. and E.Z.; software, G.L.; validation, G.L.; formal analysis, G.L., E.Z.; investigation, G.L., E.Z.; resources, G.L.; data curation, G.L., E.Z.; writing—original draft preparation, G.L.; writing—review and editing, G.L., E.Z.; visualization, G.L., E.Z.; supervision, E.Z.; project administration, G.L., E.Z.; funding acquisition, G.L. and E.Z. All authors have read and agreed to the published version of the manuscript.

Funding: This research was funded by University of L'Aquila.

Acknowledgments: Grazia Leonzio would like to thank the University of L'Aquila for funding this work.

Conflicts of Interest: The authors declare no conflict of interest.

Nomenclature

ANOVA	analysis of variance
APEA	aspen process economic analyzer
[Amim][Tf ₂ N]	1-Allyl-3-methylimidazolium bis(trifluoromethylsulfonyl)imide
[bmim][Ac]	1-butyl-3-methylimidazolium acetate
[bmim][BF ₄]	1-butyl-3-methylimidazolium tetrafluoroborate
[bmim][PF ₆]	1-Butyl-3-methylimidazolium hexafluorophosphate
[bmim][MS]	1-butyl-3-methyl imidazolium methylsulfonate
[Bpy][BF ₄]	N-butylpyridinium tetrafluoroborate
[Bmpy][NTf ₂]	Bis(trifluoromethylsulfonyl)imide (NTf ₂)
[C ₁₀ mim][TfO]	1-decyl-3-methylimidazolium trifluoromethanesulfonate
[C ₆ mim][TCM]	1-hexyl-3-methylimidazolium tricyanomethanide
CAPEX	capital costs (€)
CCD	central composite design
COP	Conference of the Parties
COSMO-RS	conductor-like screening model for realistic solvents
[emim][NTf ₂]	1-Ethyl-3-methylimidazolium bis(trifluoromethylsulfonyl)imide
[emim][EtSO ₄]	1-Ethyl-3-methylimidazolium ethyl sulfate
[emim][PF ₆]	1-Ethyl-3-methylimidazolium hexafluorophosphate
FCCCD	face centered central composite design
[hmim][Tf ₂ N]	1-n-hexyl-3-methylimidazolium bis(trifluoromethylsulfonyl)amide
[Hmpy][NTf ₂]	1-hexyl-3-methylpyridinium bis(trifluoromethylsulfonyl)imide
IL	ionic liquid
IUPAC	international union of pure and applied chemistry
MEA	monoethanolamine
[P2228][CNPyr]	octyltriethylphosphonium 2-(cyano)pyrrolide
[P66614][CNPyr]	trihexyl(tetradecyl)phosphonium 2-cyanopyrrolide
OPEX	operating costs (€/year)
RSM	response surface methodology
UNIFAC	universal functional activity coefficient

References

1. De Riva, J.; Ferro, V.; Moya, C.; Stadtherr, M.A.; Brennecke, J.F.; Palomar, J. Aspen Plus supported analysis of the post-combustion CO₂ capture by chemical absorption using the [P2228][CNPyrr] and [P66614][CNPyrr]AHA Ionic Liquids. *Int. J. Greenh. Gas Control* **2018**, *78*, 94–102. [[CrossRef](#)]
2. Valencia-Marquez, D.; Flores-Tlacuahuac, A.; Vasquez-Medrano, R. An optimization approach for CO₂ capture using ionic liquids. *J. Clean. Prod.* **2017**, *168*, 1652–1667. [[CrossRef](#)]
3. Lu, J.-G.; Ge, H.; Chen, Y.; Ren, R.-T.; Xu, Y.; Zhao, Y.-X.; Zhao, X.; Qian, H. CO₂ capture using a functional protic ionic liquid by membrane absorption. *J. Energy Inst.* **2017**, *90*, 933–940. [[CrossRef](#)]
4. Jakobsen, J.; Roussanaly, S.; Anantharaman, R. A techno-economic case study of CO₂ capture, transport and storage chain from a cement plant in Norway. *J. Clean. Prod.* **2017**, *144*, 523–539. [[CrossRef](#)]
5. Tan, Y.; Nookuea, W.; Li, H.; Thorin, E.; Yan, J. Property impacts on Carbon Capture and Storage (CCS) processes: A review. *Energy Convers. Manag.* **2016**, *118*, 204–222. [[CrossRef](#)]
6. Tola, V.; Pettinau, A. Power generation plants with carbon capture and storage: A techno-economic comparison between coal combustion and gasification technologies. *Appl. Energy* **2014**, *113*, 1461–1474. [[CrossRef](#)]
7. Ramezani, R.; Mazinani, S.; Di Felice, R.; Darvishmanesh, S.; Van Der Bruggen, B. Selection of blended absorbents for CO₂ capture from flue gas: CO₂ solubility, corrosion and absorption rate. *Int. J. Greenh. Gas Control.* **2017**, *62*, 61–68. [[CrossRef](#)]
8. Osagie, E.; Biliyok, C.; Di Lorenzo, G.; Hanak, D.P.; Manović, V. Techno-economic evaluation of the 2-amino-2-methyl-1-propanol (AMP) process for CO₂ capture from natural gas combined cycle power plant. *Int. J. Greenh. Gas Control.* **2018**, *70*, 45–56. [[CrossRef](#)]
9. Ma, T.; Wang, J.; Du, Z.; Abdeltawab, A.A.; Al-Enizi, A.M.; Chen, X.; Yu, G. A process simulation study of CO₂ capture by ionic liquids. *Int. J. Greenh. Gas Control.* **2017**, *58*, 223–231. [[CrossRef](#)]
10. Huang, B.; Xu, S.; Gao, S.; Liu, L.; Tao, J.; Niu, H.; Cai, M.; Cheng, J. Industrial test and techno-economic analysis of CO₂ capture in Huaneng Beijing coal-fired power station. *Appl. Energy* **2010**, *87*, 3347–3354. [[CrossRef](#)]
11. Babamohammadi, S.; Shamiri, A.; Aroua, M.K. A review of CO₂ capture by absorption in ionic liquid-based solvents. *Rev. Chem. Eng.* **2015**, *31*, 383–412. [[CrossRef](#)]
12. Freemantle, M. *An Introduction to Ionic Liquids*; Royal Society of Chemistry: Cambridge, UK, 2010.
13. Karunanithi, A.T.; Mehrkesh, A. Computer-aided design of tailor-made ionic liquids. *AIChE J.* **2013**, *59*, 4627–4640. [[CrossRef](#)]
14. Vijayaraghavan, R.; Oncsik, T.; Mitschke, B.; Macfarlane, D.R. Base-rich diamino protic ionic liquid mixtures for enhanced CO₂ capture. *Sep. Purif. Technol.* **2018**, *196*, 27–31. [[CrossRef](#)]
15. Lei, Z.; Dai, C.; Chen, B. ChemInform Abstract: Gas Solubility in Ionic Liquids. *Chem. Rev.* **2014**, *45*, 1289–1326. [[CrossRef](#)]
16. Luo, X.; Wang, C. The development of carbon capture by functionalized ionic liquids. *Curr. Opin. Green Sustain. Chem.* **2017**, *3*, 33–38. [[CrossRef](#)]
17. Ma, Y.; Gao, J.; Wang, Y.; Hu, J.; Cui, P. Ionic liquid-based CO₂ capture in power plants for low carbon emissions. *Int. J. Greenh. Gas Control* **2018**, *75*, 134–139. [[CrossRef](#)]
18. Zhou, L.; Fan, J.; Shang, X.; Wang, J. Solubilities of CO₂, H₂, N₂ and O₂ in ionic liquid 1-n-butyl-3-methylimidazolium heptafluorobutylate. *J. Chem. Thermodyn.* **2013**, *59*, 28–34. [[CrossRef](#)]
19. Palgunadi, J.; Kang, J.E.; Nguyen, D.Q.; Kim, J.H.; Min, B.K.; Lee, S.D.; Kim, H.; Kim, H.S. Solubility of CO₂ in dialkylimidazolium dialkylphosphate ionic liquids. *Thermochim. Acta* **2009**, *494*, 94–98. [[CrossRef](#)]
20. Revelli, A.-L.; Mutelet, F.; Jaubert, J.-N. High carbon dioxide solubilities in imidazolium-based ionic liquids and in poly(ethyleneglycol) dimethyl ether. *J. Phys. Chem. B* **2010**, *114*, 12908–12913. [[CrossRef](#)]
21. Hasib-Ur-Rahman, M.; Siaj, M.; Larachi, F. Ionic liquids for CO₂ capture—Development and progress. *Chem. Eng. Process.* **2010**, *49*, 313–322. [[CrossRef](#)]
22. Wappel, D.; Gronald, G.; Kalb, R.; Draxler, J. Ionic liquids for post-combustion CO₂ absorption. *Int. J. Greenh. Gas Control.* **2010**, *4*, 486–494. [[CrossRef](#)]
23. Zhang, J.; Sun, J.; Zhang, X.; Zhao, Y.; Zhang, S. The recent development of CO₂ fixation and conversion by ionic liquid. *Greenh. Gases Sci. Technol.* **2011**, *1*, 142–159. [[CrossRef](#)]

24. Brennecke, J.F.; Maginn, E.J. Ionic liquids: Innovative fluids for chemical processing. *AIChE J.* **2001**, *47*, 2384–2389. [[CrossRef](#)]
25. Bara, J.E.; Carlisle, T.K.; Gabriel, C.J.; Camper, D.; Finotello, A.; Gin, D.L.; Noble, R.D. Guide to CO₂ separations in imidazolium-based room-temperature ionic liquids. *Ind. Eng. Chem. Res.* **2009**, *48*, 2739–2751. [[CrossRef](#)]
26. Farahipour, R.; Mehrkesh, A.; Karunanithi, A.T. A systematic screening methodology towards exploration of ionic liquids for CO₂ capture processes. *Chem. Eng. Sci.* **2016**, *145*, 126–132. [[CrossRef](#)]
27. Huang, Y.; Zhang, X.; Zhang, X.; Dong, H.; Zhang, S. Thermodynamic Modeling and Assessment of Ionic Liquid-Based CO₂ Capture Processes. *Ind. Eng. Chem. Res.* **2014**, *53*, 11805–11817. [[CrossRef](#)]
28. Mumford, K.A.; Mirza, N.R.; Stevens, G.W. Review: Room Temperature Ionic Liquids and System Designs for CO₂ Capture. *Energy Procedia* **2017**, *114*, 2671–2674. [[CrossRef](#)]
29. Zhai, H.; Rubin, E.S. Technical and Economic Assessments of Ionic Liquids for Pre-Combustion CO₂ Capture at IGCC Power Plants. *Energy Procedia* **2017**, *114*, 2166–2172. [[CrossRef](#)]
30. Liu, X.; Huang, Y.; Zhao, Y.; Gani, R.; Zhang, X.; Zhang, S. Ionic Liquid Design and Process Simulation for Decarbonization of Shale Gas. *Ind. Eng. Chem. Res.* **2016**, *55*, 5931–5944. [[CrossRef](#)]
31. Zhao, Y.; Gani, R.; Afzal, R.M.; Zhang, X.; Zhang, S. Ionic liquids for absorption and separation of gases: An extensive database and a systematic screening method. *AIChE J.* **2017**, *63*, 1353–1367. [[CrossRef](#)]
32. Liu, X.; Zhou, T.; Zhang, X.; Zhang, S.; Liang, X.; Gani, R.; Kontogeorgis, G.M. Application of COSMO-RS and UNIFAC for ionic liquids based gas separation. *Chem. Eng. Sci.* **2018**, *192*, 816–828. [[CrossRef](#)]
33. Liu, X.; Chen, Y.; Zeng, S.; Zhang, X.; Zhang, S.; Liang, X.; Gani, R.; Kontogeorgis, G.M. Structure optimization of tailored ionic liquids and process simulation for shale gas separation. *AIChE J.* **2019**, *66*, 16794. [[CrossRef](#)]
34. Zhang, Y.; Ji, X.; Xie, Y.; Lu, X. Screening of conventional ionic liquids for carbon dioxide capture and separation. *Appl. Energy* **2016**, *162*, 1160–1170. [[CrossRef](#)]
35. Mota-Martinez, M.; Brandl, P.; Hallett, J.P.; Mac Dowell, N. Challenges and opportunities for the utilisation of ionic liquids as solvents for CO₂ capture. *Mol. Syst. Des. Eng.* **2018**, *3*, 560–571. [[CrossRef](#)]
36. Shiflett, M.B.; Drew, D.W.; Cantini, R.A.; Yokozeki, A. Carbon Dioxide Capture Using Ionic Liquid 1-Butyl-3-methylimidazolium Acetate. *Energy Fuels* **2010**, *24*, 5781–5789. [[CrossRef](#)]
37. Basha, O.M.; Keller, M.J.; Luebke, D.R.; Resnik, K.P.; Morsi, B. Development of a Conceptual Process for Selective CO₂ Capture from Fuel Gas Streams Using [hmim][Tf₂N] Ionic Liquid as a Physical Solvent. *Energy Fuels* **2013**, *27*, 3905–3917. [[CrossRef](#)]
38. Basha, O.M.; Heintz, Y.J.; Keller, M.J.; Luebke, D.R.; Resnik, K.P.; Morsi, B. Development of a Conceptual Process for Selective Capture of CO₂ from Fuel Gas Streams Using Two TEGO Ionic Liquids as Physical Solvents. *Ind. Eng. Chem. Res.* **2014**, *53*, 3184–3195. [[CrossRef](#)]
39. De Riva, J.; Suarez-Reyes, J.; Moreno, D.; Díaz, I.; Ferro, V.; Palomar, J. Ionic liquids for post-combustion CO₂ capture by physical absorption: Thermodynamic, kinetic and process analysis. *Int. J. Greenh. Gas Control* **2017**, *61*, 61–70. [[CrossRef](#)]
40. Nguyen, T.B.H.; Zondervan, E. Ionic Liquid as a Selective Capture Method of CO₂ from Different Sources: Comparison with MEA. *ACS Sustain. Chem. Eng.* **2018**, *6*, 4845–4853. [[CrossRef](#)]
41. Taheri, M.; Dai, C.; Lei, Z.; Zhigang, L. CO₂ capture by methanol, ionic liquid, and their binary mixtures: Experiments, modeling, and process simulation. *AIChE J.* **2018**, *64*, 2168–2180. [[CrossRef](#)]
42. Zacchello, B.; Oko, E.; Wang, M.; Fethi, A. Process simulation and analysis of carbon capture with an aqueous mixture of ionic liquid and monoethanolamine solvent. *Int. J. Coal Sci. Technol.* **2016**, *4*, 25–32. [[CrossRef](#)]
43. Yang, J.; Yu, X.; Yan, J.; Tu, S.-T. CO₂ Capture Using Amine Solution Mixed with Ionic Liquid. *Ind. Eng. Chem. Res.* **2014**, *53*, 2790–2799. [[CrossRef](#)]
44. Taimoor, A.A.; Al-Shahrani, S.; Muhammad, A. Ionic Liquid (1-Butyl-3-Methylimidazolium Methane Sulphonate) Corrosion and Energy Analysis for High Pressure CO₂ Absorption Process. *Processes* **2018**, *6*, 45. [[CrossRef](#)]
45. Xie, Y.; Zhang, Y.; Lu, X.; Ji, X. Energy consumption analysis for CO₂ separation using imidazolium-based ionic liquids. *Appl. Energy* **2014**, *136*, 325–335. [[CrossRef](#)]
46. Zubeir, L.F.; Lacroix, M.H.; Meuldijk, J.; Kroon, M.C.; Kiss, A.A. Novel pressure and temperature swing processes for CO₂ capture using low viscosity ionic liquids. *Sep. Purif. Technol.* **2018**, *204*, 314–327. [[CrossRef](#)]
47. Wang, Y.; Liu, X.; Kraslawski, A.; Gao, J.; Cui, P. A novel process design for CO₂ capture and H₂S removal from the syngas using ionic liquid. *J. Clean. Prod.* **2019**, *213*, 480–490. [[CrossRef](#)]

48. Zareiekordshouli, F.; Lashanizadehgan, A.; Darvishi, P. Study on the use of an imidazolium-based acetate ionic liquid for CO₂ capture from flue gas in absorber/stripper packed columns: Experimental and modeling. *Int. J. Greenh. Gas Control* **2018**, *70*, 178–192. [[CrossRef](#)]
49. Zhai, H.; Rubin, E.S. Systems Analysis of Ionic Liquids for Post-combustion CO₂ Capture at Coal-fired Power Plants. *Energy Procedia* **2014**, *63*, 1321–1328. [[CrossRef](#)]
50. Marsh, K.N.; Brennecke, J.F.; Chirico, R.D.; Frenkel, M.; Heintz, A.; Magee, J.W.; Peters, C.J.; Rebelo, L.P.N.; Seddon, K.R. Thermodynamic and thermophysical properties of the reference ionic liquid: 1-Hexyl-3-methylimidazolium bis[(trifluoromethyl)sulfonyl]amide (including mixtures). Part 1. Experimental methods and results (IUPAC Technical Report). *Pure Appl. Chem.* **2009**, *81*, 781–790. [[CrossRef](#)]
51. Widegrem, J.A.; Magee, J.W. Density, Viscosity, Speed of Sound, and Electrolytic Conductivity for the Ionic Liquid 1-Hexyl-3-methylimidazolium Bis(trifluoromethylsulfonyl)imide and Its Mixtures with Water. *J. Chem. Eng. Data* **2007**, *52*, 2331–2338. [[CrossRef](#)]
52. Billet, R.; Schultes, M. Predicting mass transfer in packed columns. *Chem. Eng. Technol.* **1993**, *16*, 1–9. [[CrossRef](#)]
53. Olujic, Z.; Seibert, A.F. Predicting the Liquid Phase Mass Transfer Resistance of Structured Packings. *Chem. Biochem. Eng. Q.* **2015**, *28*, 409–424. [[CrossRef](#)]
54. Garðarsdóttir, S.O.; Normann, F.; Skagestad, R.; Johnsson, F. Investment costs and CO₂ reduction potential of carbon capture from industrial plants—A Swedish case study. *Int. J. Greenh. Gas Control* **2018**, *76*, 111–124. [[CrossRef](#)]
55. Shiflett, M.B.; Yokozeki, A. Solubility of CO₂ in Room Temperature Ionic Liquid [hmim][Tf₂N]. *J. Phys. Chem. B* **2007**, *111*, 2070–2074. [[CrossRef](#)]
56. Baltus, R.E.; Culbertson, B.H.; Dai, S.; Luo, H.; DePaoli, D.W. Low-Pressure Solubility of Carbon Dioxide in Room-Temperature Ionic Liquids Measured with a Quartz Crystal Microbalance. *J. Phys. Chem. B* **2004**, *108*, 721–727. [[CrossRef](#)]
57. Kumelan, J.; Kamps, Á.P.-S.; Tuma, D.; Maurer, G. Solubility of CO₂ in the ionic liquid [hmim][Tf₂N]. *J. Chem. Thermodyn.* **2006**, *38*, 1396–1401. [[CrossRef](#)]
58. Zhang, S.; Chen, Y.; Ren, R.X.-F.; Zhang, Y.; Zhang, J.; Zhang, X. Solubility of CO₂ in Sulfonate Ionic Liquids at High Pressure. *J. Chem. Eng. Data* **2005**, *50*, 230–233. [[CrossRef](#)]
59. Ren, W.; Sensenich, B.; Scurto, A.M. High-pressure phase equilibria of {carbon dioxide (CO₂) + n-alkyl-imidazolium bis(trifluoromethylsulfonyl)amide} ionic liquids. *J. Chem. Thermodyn.* **2010**, *42*, 305–311. [[CrossRef](#)]
60. Valderrama, J.O.; Rojas, R.E. Critical Properties of Ionic Liquids. Revisited. *Ind. Eng. Chem. Res.* **2009**, *48*, 6890–6900. [[CrossRef](#)]
61. Ghazani, S.H.H.N.; Baghban, A.; Mohammadi, A.H.; Habibzadeh, S. Absorption of CO₂-rich gaseous mixtures in ionic liquids: A computational study. *J. Supercrit. Fluids* **2018**, *133*, 455–465. [[CrossRef](#)]
62. Li, H.; Yang, D. Modified α Function for the Peng-Robinson Equation of State To Improve the Vapor Pressure Prediction of Non-hydrocarbon and Hydrocarbon Compounds. *Energy Fuels* **2011**, *25*, 215–223. [[CrossRef](#)]
63. Privat, R.; Jaubert, J.-N. Thermodynamic Models for the Prediction of Petroleum-Fluid Phase Behaviour. In *Crude Oil Emulsions—Composition Stability and Characterization*; IntechOpen: London, UK, 2012; pp. 71–106.
64. Alvarez, V.; Aznar, M. Thermodynamic modeling of vapor–liquid equilibrium of binary systems ionic liquid + supercritical {CO₂ or CHF₃} and ionic liquid + hydrocarbons using Peng-Robinson equation of state. *J. Chin. Inst. Chem. Eng.* **2008**, *39*, 353–360. [[CrossRef](#)]
65. Ali, E.; Alnashef, I.M.; Ajbar, A.; Mulyono, S.; Hizaddin, H.F.; Hadj-Kali, M.K. Determination of cost-effective operating condition for CO₂ capturing using 1-butyl-3-methylimidazolium tetrafluoroborate ionic liquid. *Korean J. Chem. Eng.* **2013**, *30*, 2068–2077. [[CrossRef](#)]
66. Young, A.F.; Pessoa, F.L.P.; Ahón, V.R.R. Comparison of 20 Alpha Functions Applied in the Peng–Robinson Equation of State for Vapor Pressure Estimation. *Ind. Eng. Chem. Res.* **2016**, *55*, 6506–6516. [[CrossRef](#)]
67. Box, G.E.P.; Wilson, K.B. On the Experimental Attainment of Optimum Conditions. *J. R. Stat. Soc. Ser. B Methodol.* **1951**, *13*, 1–38. [[CrossRef](#)]
68. Jaliliannosrati, H.; Amin, N.A.S.; Talebian-Kiakalaieh, A.; Noshadi, I. Microwave assisted biodiesel production from *Jatropha curcas* L. Seed by two-step in situ process: Optimization using response surface methodology. *Bioresour. Technol.* **2013**, *136*, 565–573. [[CrossRef](#)]

69. Li, Y.-X.; Xu, Q.; Qiu, Z.-Z.; Wang, Z.-Y.; Liu, X.-Y.; Shi, X.; Qiu, Z.-Z.; Qin, H.; Jia, P.-Y.; Qin, Y.; et al. Removal of NO by using sodium persulfate/limestone slurry: Modeling by response surface methodology. *Fuel* **2019**, *254*, 115612. [[CrossRef](#)]
70. Montgomery, D.C. *Design and Analysis of Experiments*; John Wiley & Sons: New York, NY, USA, 2005.
71. Sheikh, Z.; Pawar, S.; Rathod, V.K. Enhancement of rhamnolipid production through ultrasound application and response surface methodology. *Process. Biochem.* **2019**, *85*, 29–34. [[CrossRef](#)]
72. Sun, Y.; Yang, Y.; Yang, M.; Yu, F.; Ma, J. Response surface methodological evaluation and optimization for adsorption removal of ciprofloxacin onto graphene hydrogel. *J. Mol. Liq.* **2019**, *284*, 124–130. [[CrossRef](#)]
73. Yaliwal, V.S.; Banapurmath, N.R.; Gaitonde, V.N.; Malipatil, M.D. Simultaneous optimization of multiple operating engine parameters of a biodiesel-producer gas operated compression ignition (CI) engine coupled with hydrogen using response surface methodology. *Renew. Energy* **2019**, *139*, 944–959. [[CrossRef](#)]
74. Zhang, P.; Akobi, M.; Khattab, A. Recyclability/malleability of crack healable polymer composites by response surface methodology. *Compos. Part B Eng.* **2019**, *168*, 129–139. [[CrossRef](#)]
75. Ferrara, G.; Lanzini, A.; Leone, P.; Ho, M.T.; Wiley, D.E. Exergetic and exergoeconomic analysis of post-combustion CO₂ capture using MEA-solvent chemical absorption. *Energy* **2017**, *130*, 113–128. [[CrossRef](#)]



© 2020 by the authors. Licensee MDPI, Basel, Switzerland. This article is an open access article distributed under the terms and conditions of the Creative Commons Attribution (CC BY) license (<http://creativecommons.org/licenses/by/4.0/>).